of the structure as built up of coordination polyhedra, the formula of phase II may be written as: $[Sn(1)_{2/3}Er(1)_{1/3}]^{XII}Er(2)_4^{X}Rh_6^{VI}Sn(2)_4^{VI}Sn(3)_{12}^{V}Sn(4)_2^{II}$. The bonds between anion-like atoms have not been taken into account.

The structures of both phases I and II are built up of $RhSn_6$ trigonal prisms. There is only a small difference between the Sn–Rh distances in the two structures: $6\times2{\cdot}649$; and $4\times2{\cdot}645$ and $2\times2{\cdot}742$ Å, respectively. These distances are far too short to correspond to a metallic character of the bonds. The trigonal prisms are almost undistorted and have comparable Sn–Sn distances and Sn–Rh–Sn angles (see Table 4). The only difference between the two structures is in the prism arrangement and consequently in the rare-earth coordination. It is possible that the trigonal-prism configurations must play an important role in the physical properties of this class of compounds.

References

CHENAVAS, J., HODEAU, J. L., COLLOMB, A., MAREZIO, M., REMEIKA, J. P. & VANDENBERG, J. (1980). Proceedings of the International Conference on Ternary Superconductors, Lake Geneva, Wisconsin, USA.

COOPER, A. S. (1980). *Mater. Res. Bull.* **15**, 799–805.

CROMER, D. T. & LIBERMAN, D. (1970). *J. Chem. Phys.* **53**, 1891–1898.

ESPINOSA, G. P. (1980). *Mater. Res. Bull.* **15**, 791–798.

HODEAU, J. L., CHENAVAS, J., MAREZIO, M. & REMEIKA, J. P. (1980). *Solid State Commun.* **36**, 839–845.

HODEAU, J. L., MAREZIO, M., REMEIKA, J. P. & CHEN, C. H. (1982). *Solid State Commun.* **42**, 97–102.

International Tables for X-ray Crystallography (1974). Vol. IV. Birmingham: Kynoch Press.

LAMBERT, S. E., FISK, Z., HAMAKER, H. C., MAPLE, M. B., WOOLF, L. D., REMEIKA, J. P. & ESPINOSA, G. P. (1980). Proceedings of the International Conference on Ternary Superconductors, Lake Geneva, Wisconsin, USA.

OTT, H. R., ODONI, W., FISK, Z. & REMEIKA, J. P. (1980). Proceedings of the International Conference on Ternary Superconductors, Lake Geneva, Wisconsin, USA.

REMEIKA, J. P., ESPINOSA, G. P., COOPER, A. S., BARZ, H., ROWELL, J. M., MCWHAN, D. B., VANDENBERG, J. M., MONCTON, D. E., FISK, Z., WOOLF, L. D., HAMAKER, H. C., MAPLE, M. B., SHIRANE, G. & THOMLINSON, W. (1980). *Solid State Commun.* **34**, 923–926.

SHENOY, G. K., VICCARO, P. J., CASHION, J. D., NIARCHOS, D., DUNLAP, B. D., PRÖBST, F. & REMEIKA, J. P. (1980). Proceedings of the International Conference on Ternary Superconductors, Lake Geneva, Wisconsin, USA.

VANDENBERG, J. M. (1980). *Mater. Res. Bull.* **15**, 835–847.

Acta Cryst. (1984). B**40**, 38–44

An Investigation of the Electron Density in Li_3N using Compton Scattering. II*

BY PHILIP PATTISON,† NIELS K. HANSEN‡ AND JOCHEN R. SCHNEIDER

Hahn-Meitner-Institut für Kernforschung, Glienicker Strasse 100, *D*-1000 *Berlin* 39, *Federal Republic of Germany*

(*Received* 24 *September* 1982; *accepted* 12 *September* 1983)

Abstract

The results of a series of Compton-profile measurements performed on the superionic conductor Li_3N are reported. The work extends to an earlier study [Pattison & Schneider (1980). *Acta Cryst.* A**36**, 390–398] which supported an ionic model of the electronic distribution in this crystal with an $(Li^+)_3N^{3-}$ configuration. The present results delineate more precisely the evidence for anisotropy in the Compton profile and hence in its Fourier transform. A detailed investigation of the directional dependence of the Fourier-transformed Compton profile within the basal Li_2N plane has been made, and it is hoped that these measurements will provide a useful test for future calculations of the electron density in lithium nitride. In order to identify the most significant interactions some simple molecular-orbital models have been employed. These models suggest that the observed anisotropy arises from the orthogonality conditions imposed on the ionic orbitals centred on the various atomic sites, which produce distortions in the non-bonding, filled shells of electrons.

1. Introduction

The electronic structure of the ionic conductor Li_3N has been for some time a subject of dispute. Theoretical descriptions have ranged from a covalent model as suggested by Krebs (1956, 1968) and Suchet (1961) to an ideal ionic crystal (Schulz & Schwarz, 1978)

* Part I: *Acta Cryst.* (1980). A**36**, 390–398.

† Present address: Fachbereich Chemie, Universität Konstanz, D-7750 Konstanz I, Federal Republic of Germany.

‡ Present address: Laboratoire de Minéralogie et Cristallographie, Université de Nancy I, BP 239, F-54506 Vandoeuvre-Les-Nancy, France.

0108-7681/84/010038-07$01.50

built up from independent closed-shell, Li^+ and N^{3-}, ions. A possible covalent model can be constructed from sp^2 hybrid orbitals on the Li sites in the Li_2N layers (the N atoms are each coordinated by eight Li atoms, six of which are in a plane and one is above and one below the N site). The two N p orbitals in this plane can overlap with the sp^2 orbitals on the Li atoms, while the third p orbital overlaps with s or sp orbitals on the Li atoms situated between the Li_2N layers. As a starting point for the solid-state study, it is instructive to examine the results of a recent SCF–MO calculation of molecular Li_3N (Hinchliffe & Dobson, 1975). A planar geometry with a bond length of 1·746 Å yielded the minimum energy for the molecule, while a population analysis indicated that the nitrogen has a charge of −2·850 e. The difference density map between Li_3N and its ions (Li^+ and N^{3-}) shows that all outer regions of the molecule are in a negative-contour region, *i.e.* the N^{3-} ion experiences a severe contraction in forming the molecule. In addition there is a build-up of charge along the bond close to the nitrogen nucleus and an almost equal build-up on the far side of the nitrogen. Hinchliffe & Dobson (1975) conclude that, despite the large, negative charge on the nitrogen ion, the electron density rearrangements indicate that Li_3N is a long way from the ionic ideal. Although it is not easy to carry over these molecular results to the situation in the solid, it is already apparent that one must be careful with the use of the terms 'ionic' or 'covalent' when discussing the electronic structure of this system.

Recently Kerker (1981) published results of a self-consistent pseudo potential band structure calculation of lithium nitride. The pseudo charge density distribution is in good agreement with a model consisting of spherical N^{3-} ions. A further improvement in the description of the calculated charge distribution can be obtained by using an ionic charge of −2·8 e on each nitrogen ion, whereby the remaining charge is uniformly distributed throughout the large interstitial regions. The Fourier-transformed Compton profiles were also calculated from the pseudo wavefunctions, and their long-range behaviour (beyond 2 Å) displayed a pronounced directional dependence in disagreement with a simple ionic picture. The origin of these anisotropies and the comparison with new experimental data will be discussed in the present work.

The major experimental evidence to date concerning the static electron density in Li_3N has come from a number of NMR studies, of which the most recent is by Differt & Messer (1980), and an X-ray diffraction study performed by Schulz & Schwarz (1978). The recent NMR results indicate that the nitrogen ion is close to N^{3-}, although Differt & Messer (1980) also conclude that there must be a remarkable deformation of the charge distribution of the N^{3-} ion. Schulz & Schwarz (1978) concluded from their X-ray data that Li_3N is indeed an ionic crystal containing the N^{3-} ion, and pointed out that this was the first time that the existence of this particular ion had been proved by diffraction methods. Since the free N^{3-} ion is unstable, the ionic form factors were calculated by Schwarz & Schulz (1978) using the Watson-sphere model (Watson, 1958) in which the surroundings of an ion in the crystal are approximated by a hollow, charged sphere. Using the radius, r_W, of this sphere as a variable parameter, a standard structure refinement led to an optimal Watson radius of 1·39 Å. The deviations in the observed electron charge density distribution from a superposition of independent ions were also synthesized and were observed to be small, indicating that there is little interaction between neighbouring ions.

A combined analysis of the X-ray and NMR data performed by Lewis & Schwarzenbach (1981) confirmed the basic ionic picture, and also indicated that there is a contraction of the N^{3-} charge density distribution along the **c** direction. Inspection of the difference charge density (crystal calculation minus superposition of Li^+ and N^{3-} ionic charge densities determined from a Watson-sphere model) as predicted by Kerker (1981) reveals no such directional contraction of the N^{3-} ion.

The fact that Li_3N has a simple, although somewhat unusual, crystal structure together with the uncertainty related to its electronic configuration makes it an attractive compound for a Compton-scattering study. Pattison & Schneider (1980, hereafter referred to as I) have measured Compton profiles along the main axes, [001], [120], [110], of the hexagonal crystal. Compton profiles were calculated for $(Li^+)_3N^{3-}$ using wavefunctions obtained from the Watson-sphere model (Schwarz, 1979). A choice of r_W close to 1·2 Å provides a very satisfactory description of the isotropic Compton profile in Li_3N. The Compton-scattering study confirmed the ionic model of Li_3N. It was argued in I that the lower value of r_W (compared to the results of the X-ray diffraction experiment) indicated that the Watson-sphere model is too crude to provide a satisfactory description of both observables. It was suggested that overlap (two-centre) terms in the crystal, arising from the orthogonality conditions imposed on ionic orbitals, may play a greater role in the Compton profile than for the structure factors.

It was already seen in I that the three directional Compton profiles displayed a marked anisotropy which cannot be explained within the isotropic Watson-sphere model. The experimental data were also Fourier transformed to obtain the position space function, $B(\mathbf{t})$ (Pattison & Weyrich, 1979), from which it could be concluded that the major contribution to the anisotropy was associated with a correlation distance of about 2·5 Å. The long-range part of $B(\mathbf{t})$ ($t > 2$ Å) revealed a deep minimum around 3 Å in the

N–N–N direction which was completely absent in the N–Li–Li–N direction (see Fig. 6 in I). It was suggested in I that this feature could be ascribed to the effects of overlap between the diffuse anions, in analogy to a similar result already observed in LiH (Pattison & Weyrich, 1979).

The comparison made by Kerker (1981) between this experimental $B(\mathbf{t})$ and his calculation shows, in general, good agreement. Kerker concludes that the N 2*s* states remain atomic-like, while the Li 2*s* states are unoccupied. Hence the dominant crystalline effects must arise from modifications of the atomic N 2*p* states when forming the valence bands. The fact that the [120] direction between neighbouring nitrogen and lithium ions shows the worst agreement with experiment suggests that the inclusion of orthogonalization terms between the valence-band wavefunctions and the core states of the atoms may play a greater role in obtaining accurate Compton profiles than hitherto assumed. In order to clarify this point, we have now collected data along a total of six independent directions within the basal plane of lithium nitride. The objectives of the present work are twofold. We wish to present these experimental data as a criterion against which to compare solid-state calculations of the electron distribution in this crystal, and to use some simple interpretative models in order to be able to identify the principal interactions whose effects we can observe in Compton-scattering experiments.

2. Experimental methods and results

The measured Compton profile, $J_{\mathbf{K}}(p_z)$, is the projection of the target electron momentum distribution, $\rho(\mathbf{p})$, onto the experimental scattering vector **K**. A detailed description of the Compton-scattering experimental technique is given in the collection of review papers edited by Williams (1977). As an aid to the interpretation of the Compton profile, we define $B(\mathbf{t})$ to be the Fourier transform of the momentum density

$$B(\mathbf{t}) = \sum_l \int |\chi_l(\mathbf{p})|^2 \exp(-i\mathbf{p}\cdot\mathbf{t})\, d^3\mathbf{p}$$
$$= \sum \int \Psi_l^*(\mathbf{r}+\mathbf{t})\Psi_l(\mathbf{r})\, d^3\mathbf{r}, \qquad (1)$$

where we have first expressed $\rho(\mathbf{p})$ in terms of the electron momentum space wavefunctions, $\chi(\mathbf{p})$, and then carried out the Fourier transform. $B(\mathbf{t})$ is thus seen to be the sum of autocorrelation functions of the position space wavefunction, $\Psi_l(\mathbf{r})$, where the summation l runs over each electron in the atom, molecule or unit cell. It is straightforward to show that the Fourier transform of a directional Compton profile yields $B_{\mathbf{K}}(z)$, where z is parallel to the experimental scattering vector, **K**. Hence, by performing measurements of the Compton profile along a sufficient number of directions in a single crystal, it is possible to determine the three-dimensional behaviour of $B(\mathbf{t})$.

The experimental conditions under which the present data have been collected are identical to those described in I. Incident photons with an energy of 412 keV (1 eV = $1{\cdot}602 \times 10^{-19}$ J) are scattered through an angle of 165°, and the Compton peak lies at about 160 keV. A cylindrical sample (radius 3·8 mm, length 4·3 mm) with [001] parallel to the cylinder axis was used. The crystal therefore was mounted so that the scattering vector lies in the basal plane, and the crystal could then be rotated around [001] in order to have an identical sample geometry for all measurements. In addition to the data already collected along [120] and [110], profiles were measured at angles of 5 and 10° away from each of these two directions, providing a total of six Compton profiles in the plane $(u, v, 0)$. In each case a total of 5×10^6 counts was accumulated under the total profile over a period of about 4 days per measurement. Each profile was then Fourier transformed to obtain the corresponding $B_{\mathbf{K}}(z)$. The profiles were normalized to the number of electrons in the unit cell [*i.e.* $B(0) = 16{\cdot}0$] and the standard deviation on each $B_{\mathbf{K}}(z)$ was 0·007 e for all z values. Since no significant difference could be observed in the $B_{\mathbf{K}}(z)$ obtained from high- and low-energy sides of each Compton profile for $z > 2$ Å, all experimental $B_{\mathbf{K}}(z)$ were derived from the average of both sides of their respective Compton profiles. The effect of the experimental resolution on $B(\mathbf{t})$ can be represented by a Gaussian attenuation of the long-range information by a factor of 2 at 3·56 Å and by a factor of 10 at 6·49 Å. No attempt was made to remove the effect of resolution from the experimental $B_{\mathbf{K}}(z)$. Multiple-scattering effects were evaluated using a Monte Carlo procedure which indicated that 3% of the total scattering arose from multiple events. The long-range part of each $B_{\mathbf{K}}(z)$ presented here is affected only indirectly by the multiple scattering, and a simple rescaling by a factor of 1·03 corrects for this systematic error.

In order to obtain a continuous description of $B(\mathbf{t})$, the measured $B_{\mathbf{K}}(z)$ were interpolated using functions of the type $\cos(m\alpha)B_m(t)$. In this way $\cos(m\alpha)$ describes the angular dependence of $B(\mathbf{t})$ [where α is the angular coordinate in the $(u, v, 0)$ plane] while the radial dependence of each $B_m(t)$ was determined by a least-squares fit to the experimental data. The values of m are constrained by the hexagonal Laue symmetry, leading to the choice of $m = 0$, 6, 12, 18 for the first four terms. It was found that four functions, $B_m(\mathbf{t})$, were sufficient to recover adequately all experimentally observed features, and the inclusion of two higher-order functions did not materially change the result.

The variation of $B(\mathbf{t})$ within the basal plane of Li_3N is shown in Fig. 1(*a*), while the crystal structure in this plane is sketched in Fig. 1(*b*) (on the same scale).

Two of the six $B_K(z)$ from which this distribution has been derived can be seen in Fig. 6(*b*) and Fig. 6(*c*) in I. For correlation distances below 2 Å all $B_K(z)$ rise sharply to a maximum value of 16·0 at the origin as defined by the normalization. Only those regions where $B(\mathbf{t})$ lies between ±0·05 e are shown in Fig. 1(*a*). The strongest feature in the map is a pronounced minimum of −0·05 at about 3 Å, which can be compared with the statistical error of 0·007. We are therefore able to observe an anisotropy in $B(\mathbf{t})$ which is less than 1% of the peak height, but which is still more than five times the standard deviation.

The Compton data presented here show that the minimum in $B(\mathbf{t})$ along the N–N direction extends over a broad angular range covering most of the basal plane. Only in a narrow channel close to the N–Li direction do we find a positive feature extending well beyond 3 Å. Although the experimental resolution suppresses the long-range information in $B(\mathbf{t})$, the map shown in Fig. 1(*a*) also indicates that the minimum around 3 Å is followed by a secondary peak at 4 Å which likewise has a very wide angular range. The details of this long-range structure are almost lost in the experimental uncertainty.

3. Discussion

The ionic picture provides a reasonable starting point for a description of Li_3N (see I). We shall therefore use the linear combination of atomic orbitals (LCAO) approach in which the basis functions (usually the free-ion wavefunctions) are orthogonalized to each other symmetrically [see, for example, Löwdin (1956) or Calais (1975)]. This localized approach to the description of the electronic states in a solid has been emphasized in recent calculations of the mutually orthogonal Wannier functions [see, for example, Kane & Kane (1978)]. The calculation of the Compton profiles by an LCAO method in ionic crystals has been described by Aikala, Jokela & Mansikka (1973) and further discussed in ch. 6 of the review edited by Williams (1977). The orthogonalization of the basis functions will introduce correlations between the functions centred on different sites and, as pointed out by Weyrich, Pattison & Williams (1979), one can expect that the autocorrelation function, $B(\mathbf{t})$, will be particularly sensitive to these effects.

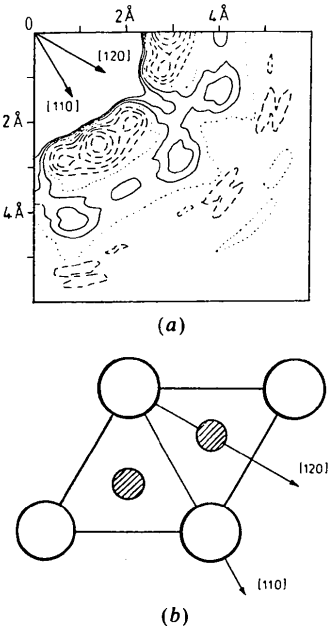

Fig. 1. (*a*) the experimental $B(\mathbf{t})$ in the basal plane of Li_3N; negative contours (broken lines) and positive contours (continuous lines) are given at intervals of 0·01 e; the experimental error is less than one contour. (*b*) A sketch of part of the Li_3N lattice in the same plane as (*a*) on the same position scale; large circles represent the N and small circles the Li atoms.

In order to calculate $B(\mathbf{t})$ for a two-centre molecular orbital (MO), one can use the prescription given by Weyrich *et al.* (1979) in their study of the Fourier analysis of the Compton profile of atoms and molecules. From equation (30) of Weyrich *et al.* (1979) we see that

$$\begin{aligned} B(\mathbf{t}) = [2(1 \pm S_{ij})]^{-1}\{&B_i(\mathbf{t}) + B_j(\mathbf{t}) \\ &\pm \int \varphi_i^*(\mathbf{s}+\mathbf{t}+\mathbf{R})\varphi_j(\mathbf{s})\,\mathrm{d}^3\mathbf{s} \\ &\pm \int \varphi_j^*(\mathbf{s}+\mathbf{t}-\mathbf{R})\varphi_i(\mathbf{s})\,\mathrm{d}^3\mathbf{s}\}, \end{aligned} \tag{2}$$

where φ_i and φ_j are atomic orbitals centred on sites i and j which are $\mathbf{R}$ apart, and S_{ij} is the overlap integral between φ_i and φ_j. $B_i(\mathbf{t})$ and $B_j(\mathbf{t})$ are the $B(\mathbf{t})$ resulting from the atomic orbitals on atoms i and j, respectively. The choice of sign in (2) determines whether the MO configuration is bonding or antibonding. It is clear from (2) that it is possible to separate the total MO $B(\mathbf{t})$ into atomic (one-centre) and molecular (two-centre) terms. Where there are filled atomic shells on the various crystal sites, the sum of the one-centre terms will make no contribution to the anisotropy. Therefore one can look for possible sources of anisotropy in a crystal $B(\mathbf{t})$ by examining various two-centre bonding or antibonding interactions between different pairs of neighbours in the lattice.

Close inspection of (2) reveals that the problem of orthogonalization can be approached directly within this MO scheme. If we take an equal mixture of bonding and antibonding terms in (2) in order to represent the formation of MO's between two filled-shell ions, the total $B(\mathbf{t})$ can be written

$$\begin{aligned} B(\mathbf{t}) &= [1 - S_{ij}^2]^{-1}\{B_i(\mathbf{t}) + B_j(\mathbf{t}) \\ &\quad - S_{ij}[\int \varphi_i^*(\mathbf{s}+\mathbf{t}+\mathbf{R})\varphi_j(\mathbf{s})\,\mathrm{d}^3\mathbf{s} \\ &\quad + \int \varphi_j^*(\mathbf{s}+\mathbf{t}+\mathbf{R})\varphi_i(\mathbf{s})\,\mathrm{d}^3\mathbf{s}]\} \\ &= [1 - S_{ij}^2]^{-1}\{B_i(\mathbf{t}) + B_j(\mathbf{t}) - S_{ij}B_{ij}(\mathbf{t})\}. \end{aligned} \tag{3}$$

Hence $B(\mathbf{t})$ for a completely filled MO is seen to

contain not only the atomic terms, $B_i(\mathbf{t})$ and $B_j(\mathbf{t})$, but also an antibonding, two-centre term, $B_{ij}(\mathbf{t})$, which is proportional to the overlap integral, S_{ij}. This antibonding term, weighted by the overlap integral, provides the necessary orthogonalization between the filled atomic orbitals φ_i and φ_j. A similar statement has been made by Coulson (1968) who pointed out that the total bond order for He_2, for example, is $-2S/(1-S^2)$, where the overlap integral S will be small and positive. Hence the bond order for completely filled MO shells will generally be negative, implying that there will be a net antibonding, repulsive interaction between the two atoms. This repulsion is seen in the crystal as a contraction of the electron density distribution *via* the orthogonalization effect. Therefore, in order to represent the major effects of wavefunction orthogonalization in the crystal, it is simply necessary for us to evaluate the directional dependence of antibonding interactions between the various orbitals φ_i and φ_j, taking into account the fact that the contribution of any particular orbital pair will be weighted according to their overlap integral, S_{ij}, as shown in (3). In this way we can identify the anisotropy in $B(\mathbf{t})$ which would arise from placing spherical ions within the crystal environment.

We will now evaluate the two-centre correlation function $B_{ij}(\mathbf{t})$ as defined in (3) using a minimum basis set of Slater-type orbitals (STO's) with orbital exponents chosen as follows: Li(1*s*) = 2·69, N(2*s*) = N(2*p*) = 1·60. For Li(1*s*) the exponent corresponds to the Slater-rule value, while for N the orbitals have been allowed to relax somewhat from the Slater-rule values for N in order to simulate the situation in the N^{3-} ion. When evaluating the overlap integrals between the *s* and *p* STO's appearing in (3), the overlap formulae as given by Roothaan (1951) proved to be particularly helpful.

Considering first the N–N interaction, we construct an sp^2 hybrid orbital on the two nitrogen sites, each oriented with its lobe pointing towards its neighbour. Although many other relative orientations could be taken into account, the chosen configuration should have the largest overlap integral, S_{ij}, and hence contribute the most significant *orthogonalization* term to the total MO $B(\mathbf{t})$. We show in Fig. 2 the *antibonding* $B_{ij}(t)$ for **t** lying along the N–N axis and also 30° away from this direction (corresponding to the crystal vectors [110] and [120], respectively) for an interatomic distance of R equal to 3·649 Å. If we consider the behaviour of $B_{ij}(\mathbf{t})$ for $t > 2$ Å, *i.e.* beyond the range where the one-centre terms dominate $B(\mathbf{t})$, it appears that this N–N antibonding term can account very well for the pronounced minimum between 2 and 3 Å seen in the experiment. The fact that this is a broad angular feature in the experiment, rather than a local depression along [110], is consistent with the diffuse nature of the 2*s* and 2*p* orbitals on the nitrogen sites. The long-range peak in the experimental $B(\mathbf{t})$ around 4 Å can also be explained from this N–N interaction, as seen in Fig. 2. However, this term alone can definitely not account for the positive feature at 3 Å in the [120] direction observed experimentally, indicating that we must examine other possible overlap terms for this crystal. In Table 1 we show the overlap integrals between various orbitals on neighbouring ions. The Watson-sphere model wavefunctions from Schwarz & Schulz (1978) for N 2*s* and N 2*p* were used. It is clear that the overlaps between Li 1*s* and the nitrogen *L*-shell orbitals are of the same order as the nitrogen–nitrogen overlaps. We must therefore also consider the influence of the N–Li orthogonalization term. In this case the maximum overlap integral will occur for an sp^2 orbital on the N with its lobe directed towards the 1*s* orbital of the neighbouring Li. In Fig. 3 we present the antibonding $B_{ij}(\mathbf{t})$ for this configuration for an interatomic distance of 2·107 Å. The correlation function has been calculated along the N–Li axis and 30° away from this axis (corresponding to the crystal vectors [120] and [110], respectively). In the [110] direction there is again a minimum which will reinforce the strong negative feature arising from the N–N antibonding. However, we see from Fig. 3 that there is indeed a peak along [120] between 2 and 4 Å arising from the N–Li term. The fact that this peak is a

Table 1. *Overlap between orbitals on nearest-neighbour ions in the* (0, 0, 1) *plane*

p_σ denotes the *p* orbital pointing in the direction of the neighbour considered, p_π an orbital perpendicular to this direction. The nitrogen orbitals are from a Watson-sphere calculation with a Watson radius of 1·4 Å, and the Li 1*s* from a free-ion calculation (Aikala, 1980).

		N 2*s*	N $2p_\sigma$	N $2p_\pi$
Li	1*s*	0·035	0·113	—
N	2*s*	0·012	0·059	—
N	$2p_\sigma$	0·059	0·117	—
N	$2p_\pi$	—	—	0·034

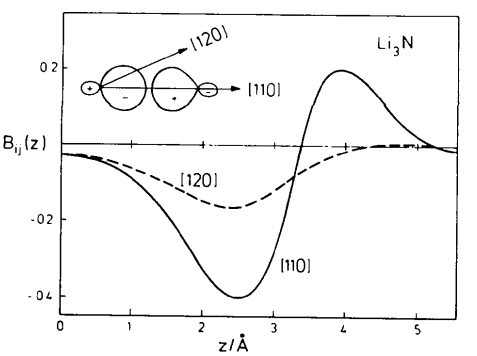

Fig. 2. The two-centre correlation function between two antibonding sp^2 orbitals on neighbouring nitrogen sites in the Li_3N lattice. The results are given for relative displacements either along the N–N axis, [110], or 30° away, [120].

localized feature in the experimental $B(\mathbf{t})$ is consistent with the compact nature of the Li 1s electron distribution.

The qualitative features observed in the experimental $B(\mathbf{t})$ presented in Fig. 1(a) can be accounted for in terms of the adaptation of the ions to the neighbouring Li and N in the basal plane. Unfortunately, since the isotropic, one-centre terms dominate $B(\mathbf{t})$ at distances below about 2 Å, we cannot judge the accuracy of our simple model at short range on the basis of the experimental results as present so far. However, we can examine the difference between the $B(\mathbf{t})$ measured in two different crystallographic directions in which the isotropic terms should cancel. This has already been done in I for the directions [120] and [110] (Fig. 5 of I), and we can now compare this difference curve with the predictions of the MO model. The contributions to the anisotropy arising from both N–N and N–Li orthogonalization shown in Figs. 2 and 3 have been added together (the overlap integrals for the two configurations being almost identical) and the experimental resolution taken into account by multiplying by a Gaussian (as described in § 2). The theoretical anisotropy in $B(\mathbf{t})$ was then scaled to give the same maximum amplitude as the experimental difference curve, and the resulting comparison between theory and experiment is shown in Fig. 4. The good agreement between the shape of the experimental and theoretical difference curves confirms the interpretation of the anisotropy as arising from antibonding in which N–N and N–Li interactions are of roughly equal importance.

We have been able to account qualitatively for most of the observed directional dependence of $B(\mathbf{t})$ in the basal plane of Li_3N on the basis of a simple MO model which simulates the effects of orthogonalization within the ionic, filled-shell system. A similar approach has already proved to be successful in typical ionic crystals such as LiF and LiH (Aikala, 1979; Pattison & Weyrich, 1979). Can Li_3N thus be placed

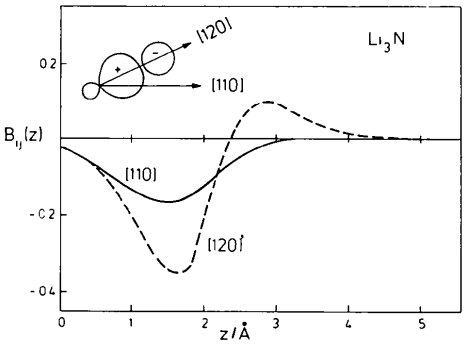

Fig. 3. The two-centre correlation function between an antibonding sp^2 orbital on the nitrogen and a 1s orbital on the neighbouring lithium site in the basal plane of Li_3N. The results are given for relative displacements either along the N–Li axis, [120], or 30° away, [110].

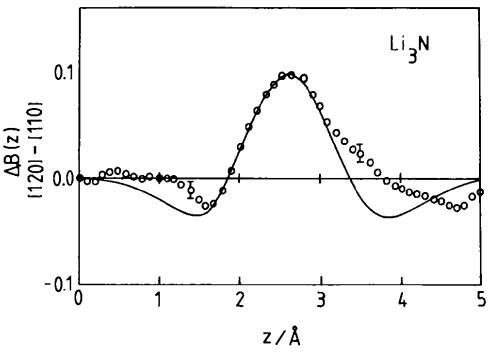

Fig. 4. The anisotropy in $B(\mathbf{t})$ between the directions [120] and [110] due to antibonding interactions between N–N and N–Li neighbours within the Li_2N layer of lithium nitride is shown by the continuous line. The experimental results (circles) have been taken from Fig. 5 of I. The amplitude of the theoretical curve has been scaled to give the same maximum anisotropy as the experiment.

in the same category? On the basis of the present experimental Compton-scattering data, the answer to this question must be affirmative. However, one must emphasize that the data set is limited both in the number of crystallographic directions which have been measured, and in the level of statistical accuracy and resolution which is achievable at present. From the point of view of the theoretical results of Kerker (1981), we have indicated possible problems met when applying the pseudopotential method to calculate Compton profiles.

We would like to thank Professor H. Schulz for supplying the single crystal of Li_3N (which was prepared at the Max-Planck-Institut für Festkörperforschung in Stuttgart), and to express our thanks to Dr O. Aikala for several useful discussions concerning the importance of orthogonality effects in Compton profiles. The financial support of the Deutsche Forschungsgemeinschaft is gratefully acknowledged.

References

AIKALA, O. (1979). *Philos. Mag.* **B39**, 437–446.
AIKALA, O. (1980). Private communication.
AIKALA, O., JOKELA, V. & MANSIKKA, K. (1973). *J. Phys. C*, **6**, 1116–1124.
CALAIS, J.-L. (1975). *Int. J. Quantum Chem. Symp.* **9**, 497–518.
COULSON, C. A. (1968). *Mol. Phys.* **15**, 317–320.
DIFFERT, K. & MESSER, R. (1980). *J. Phys. C*, **13**, 717–729.
HINCHLIFFE, A. & DOBSON, J. C. (1975). *Theor. Chim. Acta*, **39**, 17–24.
KANE, O. E. & KANE, B. (1978). *Phys. Rev. B*, **17**, 2691–2704.
KERKER, G. (1981). *Phys. Rev. B*, **23**, 6312–6318.
KREBS, H. (1956). *Acta Cryst.* **9**, 95–108.
KREBS, H. (1968). *Grundzüge der anorganischen Kristallchemie*, pp. 247–248. Stuttgart: Ferdinand Enke Verlag.
LEWIS, J. & SCHWARZENBACH, D. (1981). *Acta Cryst.* **A37**, 507–510.
LÖWDIN, P. O. (1956). *Adv. Phys.* **5**, 1–171.
PATTISON, P. & SCHNEIDER, J. R. (1980). *Acta Cryst.* **A36**, 390–398.

PATTISON, P. & WEYRICH, W. (1979). *J. Phys. Chem. Solids*, **40**, 213–222.
ROOTHAAN, C. C. J. (1951). *J. Chem. Phys.* **19**, 1445–1458.
SCHULZ, H. & SCHWARZ, K. (1978). *Acta Cryst.* A**34**, 999–1005.
SCHWARZ, K. (1979). Private communication.
SCHWARZ, K. & SCHULZ, H. (1978). *Acta Cryst.* A**34**, 994–999.
SUCHET, J. P. (1961). *Acta Cryst.* **14**, 651–659.
WATSON, R. E. (1958). *Phys. Rev.* **111**, 1108–1110.
WEYRICH, W., PATTISON, P. & WILLIAMS, B. G. (1979). *Chem. Phys.* **41**, 271–284.
WILLIAMS, B. G. (1977). Editor. *Compton Scattering*. London: McGraw-Hill.

Acta Cryst. (1984). B**40**, 44–59

Structural Evolution of the One-Dimensional Organic Conductor Triethylammonium–7,7,8,8-Tetracyano-*p*-quinodimethane (1:2) [TEA–$(TCNQ)_2$] in the Temperature Range 40 to 345 K

BY ALAIN FILHOL AND MICHEL THOMAS

Institut Laue–Langevin, 156*X*, *F*-38042 *Grenoble CEDEX*, *France*

(*Received* 24 *February* 1983; *accepted* 28 *July* 1983)

Abstract

The X-ray structure of TEA–$(TCNQ)_2$ has been measured at 110, 173, 234 and 345 K, which, in addition to data in the literature, enables a detailed description of the structural evolution of the compound with temperature. The charge transfer estimated from bond lengths indicates a partial localization (0·6 and 0·4 e) of the charges, on the two independent TCNQ molecules, in the temperature range considered. The unit-cell thermal expansion has been measured in the range 156 to 367 K. An anomaly at 200–220 K was found and the related structural changes are described. Since electrical-conductivity anomalies at 200–220 K have already been reported and sometimes attributed to a metal–insulator phase transition, an attempt is thus made to interpret the temperature dependence of the stacking distances in the TCNQ columns in terms of Peierls-like lattice distortions – namely dimerization and tetramerization.

Introduction

Some years ago it was usually assumed that, in the crystalline state, TCNQ salts with a regular stacking of the TCNQ molecules were the only ones with one-dimensional (1D) metal-like properties. TCNQ salts with irregular stacking (tetrads, diads, *etc.*) were classified as semiconductors or insulators, depending on the quality of the molecular overlap in the columns. Another idea was that irregular stacking at high temperature could be the result of a 'virtual' Peierls transition, *i.e.* a Peierls transition that would have occurred above the melting point of the compound (*e.g.* Kommandeur, 1975).

In fact, this approach was too simple, and the study of 1D conductors with cationic conducting chains (cations of the TTF* family) has shown that strict regular stacking is not in itself necessary for metal-like behaviour. Similar observations have also been made for TCNQ salts [*e.g.* for MEM–$(TCNQ)_2$ by van Bodegom (1979) and for TMA–TCNQ–I by Filhol, Gallois, Laugier, Dupuis & Coulon (1982) and Gallois, Coulon, Pouget, Filhol & Dupuis (1983)]. It was thus of interest to reconsider the case of TEA–$(TCNQ)_2$, which is one of the best known TCNQ salts because large single crystals have been available for a long time.

TEA–$(TCNQ)_2$ is generally considered as a good 1D semiconductor ($\sigma_{\parallel 300\,K} \sim 5{\cdot}7\ \Omega^{-1}\ cm^{-1}$) and in fact its structure (Kobayashi, Ohashi, Marumo & Saito, 1970; Jaud, Chasseau, Gaultier & Hauw, 1974; Potworowski, 1974; Filhol, Zeyen, Chenavas, Gaultier & Delhaes, 1980) shows typical irregular tetradic stacking of the TCNQ molecules (Fig. 1). However, the temperature dependence of the longitudinal conductivity of this compound shows an anomaly at 200–220 K (see *e.g.* Brau & Farges, 1974) which is in fact a jump of one order of magnitude if the samples are small, needle-shaped single crystals (Grassi, Brau & Farges 1979; Farges, 1979). Furthermore, some authors (*e.g.* Vlasova *et al.*, 1975) have postulated that this transition is of the *metal–insulator* type while others incline towards a *semiconductor–semiconductor* mechanism.

* TTF–TCNQ: tetrathiafulvalene–TCNQ; TMA–TCNQ–I [$TMA^+.TCNQ^{2/3-}.(I_3^-)_{1/3}$]: trimethylammonium–TCNQ–iodine; MEM–$(TCNQ)_2$: ethyl(methyl)morpholinium–$(TCNQ)_2$.

0108-7681/84/010044-16$01.50